Biochimica et Biophysica Acta 1838 (2014) 1769–1776

Contents lists available at ScienceDirect

Biochimica et Biophysica Acta

journal homepage: www.elsevier.com/locate/bbamem

Comprehensive portrait of cholesterol containing oxidized membrane

Martin Štefl [a,1], Radek Šachl [a,1], Agnieszka Olżyńska [a], Mariana Amaro [a], Dariya Savchenko [b], Alexander Deyneka [b], Albin Hermetter [c], Lukasz Cwiklik [a,*], Jana Humpolíčková [a,*], Martin Hof [a]

[a] J. Heyrovský Institute of Physical Chemistry of the Academy of Sciences of the Czech Republic, v. v. i., Dolejškova 2155/3, 182 23 Prague 8, Czech Republic
[b] Institute of Physics, Academy of Sciences of the Czech Republic, v. v. i., Na Slovance 1999/2, 182 21 Prague 8, Czech Republic
[c] Institute of Biochemistry, University of Technology, Graz, Petersgasse 12/II, A-8010 Graz, Austria

ARTICLE INFO

Article history:
Received 19 November 2013
Received in revised form 30 January 2014
Accepted 12 February 2014
Available online 22 February 2014

Keywords:
Oxidized lipids
Lateral diffusion
Molecular dynamics simulations
Fluorescence correlation spectroscopy
Electron paramagnetic resonance

ABSTRACT

Biological membranes are under significant oxidative stress caused by reactive oxygen species mostly originating during cellular respiration. Double bonds of the unsaturated lipids are most prone to oxidation, which might lead to shortening of the oxidized chain and inserting of terminal either aldehyde or carboxylic group. Structural rearrangement of oxidized lipids, addressed already, is mainly associated with looping back of the hydrophilic terminal group. This contribution utilizing dual-focus fluorescence correlation spectroscopy and electron paramagnetic resonance as well as atomistic molecular dynamics simulations focuses on the overall changes of the membrane structural and dynamical properties once it becomes oxidized. Particularly, attention is paid to cholesterol rearrangement in the oxidized membrane revealing its preferable interaction with carbonyls of the oxidized chains. In this view cholesterol seems to have a tendency to repair, rather than condense, the bilayer.

1. Introduction

Unsaturated phospholipids, abundant constituents of cellular membranes, are prone to being chemically modified due to oxidative stress. Reactive oxygen species (ROS) often disrupt double bonds [1] which is then followed by insertion of oxygen atoms either to the side of the hydrophobic lipid chain in the form of hydroxides or hydroperoxides [2], or the carbon chain (typically *sn*-2) is truncated and terminated by a polar aldehyde or carboxylic group [3]. These oxidized phospholipids (oxPLs) have been related to various patho-physiologies such as inflammation [4–6] or atherosclerosis [5] just to name a few. OxPLs experience increased reactivity which may turn into further propagation of the oxidative reaction among lipids through the mitochondrial membrane, where ROS are mainly generated, to other organelles or cells. Furthermore, the insertion of an aldehyde group enables Schiff base formation [7] with amino groups in various proteins and lipids leading to significant changes of molecular properties of these moieties.

Terminating the *sn*-2 chain with a hydrophilic group is inevitably connected with structural rearrangement of the membrane since the strongly hydrophobic tail region of the membrane is no longer preferable for the oxidized chain. To minimize the unfavorable interaction, the chain has been shown to reverse out to the aqueous phase [8]. This phenomenon alters the membrane biophysics, which is the issue we would like to focus on in this manuscript.

The biophysical properties of membranes containing oxPLs have been addressed in a few papers already [8–12]. In lipid monolayers containing immiscible lipid phases, the presence of truncated phosphatidylcholines stabilizes liquid ordered domains [13]. Further, it has been shown that lipid oxidation increases partitioning of the truncated lipid into the liquid ordered phase and an increased diffusion coefficient of the oxidized moiety has been reported [11]. Molecular dynamics (MD) simulations using coarse grained Martini force field explain the altered diffusion behavior by pulling of the oxPL hydrophilic headgroups out of the DOPC headgroup region. The MD simulations further predicted that oxPLs are drug back inwards after cholesterol had been added. This was experimentally demonstrated by smearing out the difference in diffusion coefficients between the oxidized and non-oxidized lipids upon cholesterol addition [11].

While the diffusion study concentrates on the motion of the truncated lipid, here we address the physical properties of the entire single-phase membrane containing oxPLs. We investigate membrane bilayers consisting of 1-palmitoyl-2-oleoyl-sn-glycero-3-phosphocholine (POPC) where 5 to 10% of POPC molecules were replaced by 1-palmitoyl-2-glutaryl-sn-glycero-3-phosphocholine (PGPC), with oleoyl residue replaced by truncated carbon chain terminated with a carboxylic acid. By means of atomistic MD simulations, as well as experimentally, we examine the role of cholesterol showing that it fills the void space arisen upon truncation of the lipid chain. On free standing model membranes of giant unilamellar

* Corresponding authors. Tel.: +420 266053142.
E-mail addresses: martin.stefl@jh-inst.cas.cz (M. Štefl), radek.sachl@jh-inst.cs.cz (R. Šachl), agnieszka.olzynska@jh-inst.cas.cz (A. Olżyńska), mariana.amaro@jh-inst.cas.cz (M. Amaro), savchenko@fzu.cz (D. Savchenko), dejneka@fzu.cz (A. Deyneka), albin.hermetter@tugraz.at (A. Hermetter), lukasz.cwiklik@jh-inst.cas.cz (L. Cwiklik), jana.humpolickova@jh-inst.cas.cz (J. Humpolíčková), martin.hof@jh-inst.cas.cz (M. Hof).
[1] These authors contributed equally to this work.

http://dx.doi.org/10.1016/j.bbamem.2014.02.006
0005-2736/

vesicles (GUVs) we demonstrate oxidation-promoted changes in diffusion properties of individual membrane components and the effect of cholesterol in minimizing the oxidative bilayer damage. The MD simulations explain the phenomena by revealing a cholesterol population that specifically interacts with the carbonyl oxygen in the truncated lipid chain. The cholesterol carbonyl interaction with the truncated lipid is, compared to the same interaction with non-truncated lipids, further favored by better access to the carbonyl. The subtle structural membrane changes are translated to the lipid mobility characterized by the lateral diffusion coefficient or reorientation of the spin label.

2. Results

2.1. Structure of PGPC containing bilayer as obtained by MD simulations

As we would like to emphasize the role of cholesterol in oxidized membranes, both in simulations as well as in experiments we focus on different effects of cholesterol in oxidized and non-oxidized membranes. Generally, it is accepted that cholesterol causes lateral shrinking of the fluid phospholipid bilayer accompanied by increase of its thickness. This ordering and increased lateral compactness is commonly represented by a reduced area per lipid (APL). Our simulations show a lower cholesterol-dependent drop in APL in the POPC bilayer with 9% POPC replaced by PGPC than in a pure POPC bilayer (a drop of 4.7% and 6.1%, respectively). This suggests that the cholesterol action is suppressed in the oxidized membrane, which is in agreement with the experiments that will follow. APL is however a global parameter that does not directly explain what happens at the level of individual lipid molecules. Therefore, we will now concentrate on the atomistic description of the bilayer to comprehend the origin of the changes.

The main structural effect of the oxidized PGPC lipids' presence in the POPC membrane is the reorientation of truncated *sn*-2 chains of PGPC resulting in the occurrence of their termini at the lipid/water interface. As evident from density profiles presented in Fig. 2, oxygen atoms of carboxylate groups at the termini of PGPC *sn*-2 penetrate into the POPC headgroup region and reside between phosphate and choline groups of POPC (the protrusion of the carboxylate groups of PGPC is also visible in the simulation snapshot shown in Fig. S1 in the Supporting information). Hence, the truncated PGPC chains protrude from the membrane into the water phase. This is further evidenced by the distribution of *sn*-2 tilt-angles shown in Fig. 3A which demonstrate that the majority of the truncated chains of PGPC are reoriented towards the water phase and none of them is directed towards the membrane core. This is in accord with previous simulations and experimental results concerning various truncated forms of oxidized phosphatidylcholines [8–10,14]. As was discussed in those studies, reorientation of oxidized chains occurs due to the polar character of their terminal groups which prefer the well hydrated headgroup environment over the non-polar membrane core.

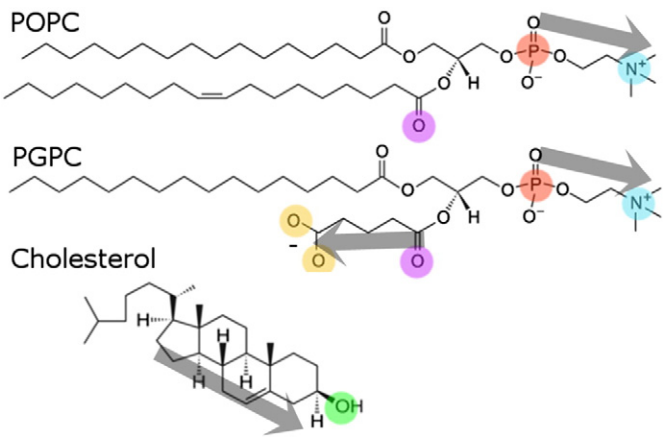

Fig. 1. Chemical structures of lipids considered in this work. The highlighted atoms and vectors are used in the analysis of structural membrane properties in MD simulations (see Figs. 2 and 3).

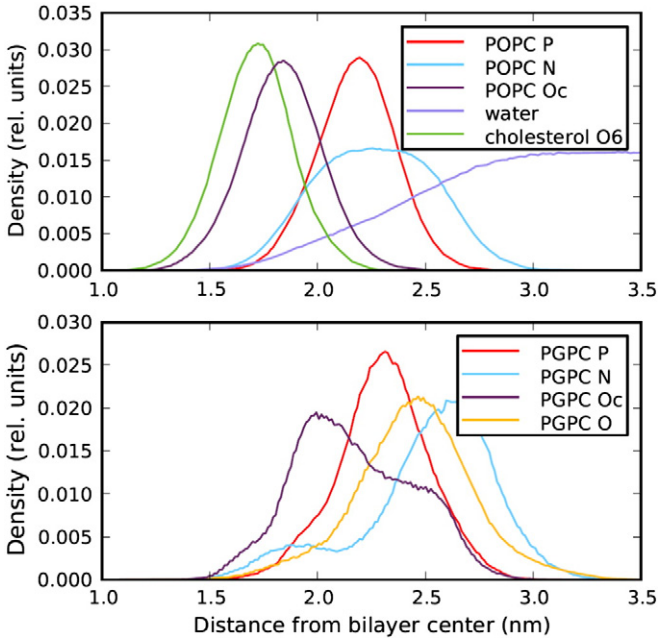

Fig. 2. Density profiles calculated across the membrane based on MD simulation of the POPC + PGPC + chol (116:12:38) bilayer. The following individual membrane components are presented: carbonyl oxygen atoms in *sn*-2 chains (O_c); nitrogen atoms in choline groups (N); phosphorus atom in phosphate groups (P); oxygen atoms in carboxylate groups of the truncated *sn*-2 chain of PGPC ($O_{carboxyl}$); oxygen atoms in hydroxyl groups of cholesterol (O_3) and water. See Fig. 1 for molecular structures. All curves are normalized in order to have the same integral. Density profiles of both membrane leaflets are averaged.

A comparison of tilt-angle distributions calculated in membranes with and without cholesterol, presented in Fig. 3A, shows that the presence of cholesterol has no significant influence on the reorientation of truncated *sn*-2 chains of PGPC. With cholesterol present, most of oxidized chains are reversed and none is directed towards the membrane interior.

Furthermore we analyze in detail the position of lipid headgroups and their orientation in the membrane. In accordance with literature, our MD simulations predict that the presence of 9% of carboxyl-terminated truncated PGPC does not affect the headgroup positions of the prevailing POPC lipid molecules with respect to the membrane center [11]. In the presence of PGPC, in both cholesterol-containing and cholesterol-free bilayers, the distance of the POPC headgroup from the center of the bilayer remains unaffected (see Fig. S2). PGPC headgroups do not coexist in the same position with POPC but shift outwards from the bilayer center, probably due to the looping back of the carboxyl terminated *sn*-2 chains. The orientational freedom of headgroups, which can be associated with the width of the P-N angles distribution, is significantly higher for PGPC than for POPC (see Fig. 3B,C). This can be attributed to two effects. First, the PGPC headgroups shift from the crowded POPC headgroup region towards the water phase, where headgroups have more orientational freedom than in their typical localization. Second, the reversal of PGPC *sn*-2 chains causes many conformational changes in the PGPC molecules and hence affects also the PGPC headgroup orientation. The distribution appears to become bimodal with a population of straight-staying and flat-laying PGPC headgroups (see arrows in Fig. 3C).

When cholesterol is inserted, acyl chains in POPC become more ordered which causes POPC headgroups to shift further from the bilayer center (see Fig. S2 in the Supporting information). The presence of cholesterol has a strong effect on PGPC headgroups (see Fig. 3C). In

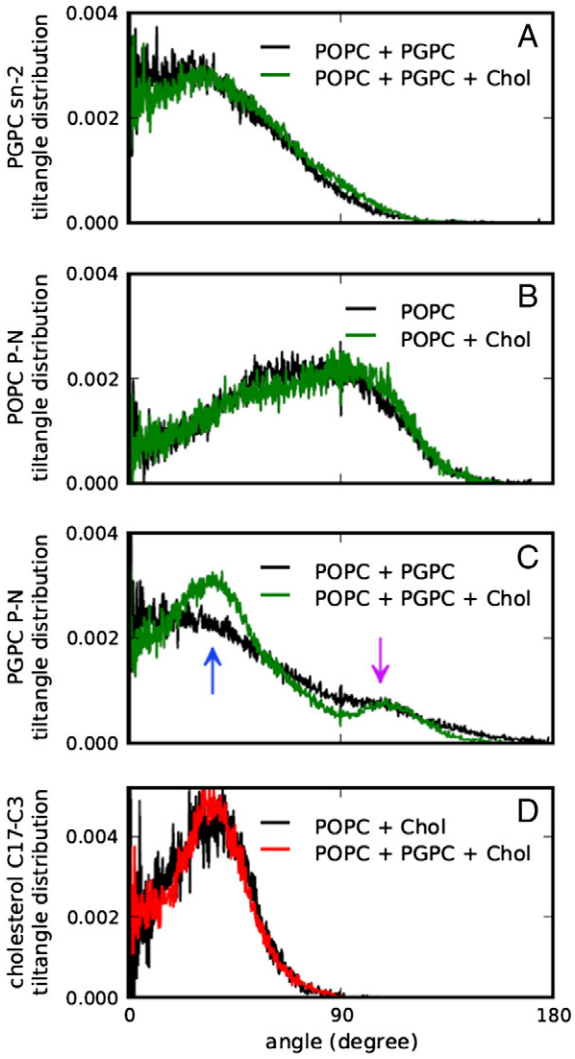

Fig. 3. Orientation of lipid molecules in simulated membranes (lipid compositions are given in the figures) probed by probability distribution of tilt-angles of selected vectors with respect to the membrane normal: *sn*-2 chain vector in PGPC (defined as the vector between the first and last carbon atoms of the chain) (A); P-N vectors in POPC and PGPC (B, C); C17–C3 vector in cholesterol (D). See Fig. 1 for schematic representation of the considered vectors in corresponding molecules. The angle value of 0° corresponds to the orientation out of the membrane, 90° — parallel to the membrane, 180° — into the membrane. In order to get probability distributions, the distributions of angles are normalized by sin (angle). In C, the arrows represent straight-staying (blue) and flat-laying (purple) PGPC headgroup orientations.

the absence of cholesterol, the distribution of P-N tilt-angles is relatively wide, hence the straight-standing and flat-laying headgroups of PGPC may easily interchange, and there is also a high population of intermediate angles. In the presence of cholesterol, the PGPC headgroup orientation becomes significantly rigidified. The tilt-angle distribution becomes bimodal resulting in the enhancement of both straight-standing and flat-laying orientations and the reduction of intermediate ones. In their study employing coarse grain MD simulations, Plochberger et al. [11] demonstrate a shift of the PGPC phosphate groups inwards the bilayer upon the addition of cholesterol. Based on the atomistic-level simulations discussed here, we attribute the changes of PGPC headgroup position in the presence of cholesterol mainly to alterations of PGPC headgroup tilt-angle.

Cholesterol orientation in oxidized and non-oxidized bilayers can be described by the distribution of C17–C3 tilt-angles (see Fig. 3D). As shown in our earlier studies, the presence of PGPC with reoriented *sn*-2 chains leads to the occurrence of void regions in the bilayer core which are typically populated by water [10]. It could be anticipated that such void spaces should lead to less rigid orientation of cholesterol than in non-oxidized POPC membrane. However, in the PGPC-containing bilayer we do not observe significant modifications of cholesterol tilt-angle distribution with respect to the non-oxidized membrane. The cholesterol tilt-angle distribution appears to be even slightly narrower in the oxidized membrane. This suggests that cholesterol may strongly interact with PGPC and thus be orientationally restricted despite the presence of the void regions formed upon reorientation of the *sn*-2 chains. This issue will be further discussed and quantified in the following section and the impact of this fact on the dynamics of the bilayer will be demonstrated.

2.2. PGPC presence reflected by large timescale dynamics: FCS measurements and MD simulations

Lateral lipid diffusion on the length scale of several hundreds of nanometers, which can be accessed by monitoring fluorescence signal changes in a diffraction limited area, occurs on the millisecond timescale. While fluorescence microscopy techniques are often used for these purposes, MD simulations cannot achieve such timescales. Therefore, here we will attempt to elucidate the experimental data in the view of the bilayer's structural properties.

As pointed out already, PGPC in the bilayer manifests itself by i) reversal of its truncated chain, ii) changes in the headgroup orientation stabilized upon cholesterol addition, and iii) a specific interaction between the carbonyl of the truncated chain and cholesterol.

The effect of cholesterol has been examined also experimentally. Cholesterol is known to have a substantial impact on the bilayer dynamics. Therefore, first we have explored the diffusion coefficient of various lipid moieties.

Particularly, we have measured the diffusion of bodipy-labeled PGPE (Bod-PGPE) and ATTO-488 labeled POPE (ATTO488-POPE), i.e. an oxidized and non-oxidized lipid, in the free-standing bilayer of giant unilamellar vesicles (GUVs) composed either of pure POPC or POPC with 5 mol% of PGPC. Thus, we have explored the diffusion in four different systems: i) non-oxidized moiety in an unperturbed bilayer, ii) oxidized moiety in an unperturbed bilayer, iii) non-oxidized moiety in a perturbed bilayer, and iv) oxidized moiety in a perturbed bilayer. As the main goal of our investigations was addressing the role of cholesterol, diffusion in the four systems of interest was observed as a function of cholesterol content. The data measured independently by 2-foci FCS and Z-scan FCS are given in Fig. 4.

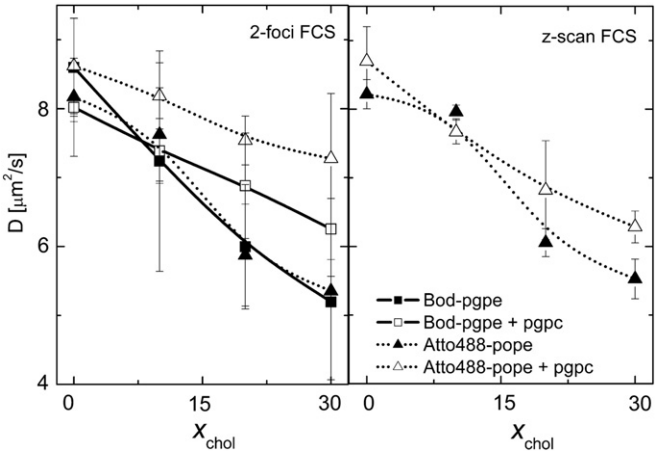

Fig. 4. Dependence of the diffusion coefficient of Bod-PGPE (squares) and Atto488-POPE (triangles) on the cholesterol content in oxidized (open squares/triangles) and non-oxidized (closed squares/triangles) membranes, measured by 2-foci FCS (left) and Z-scan FCS (right). The error bars represent the standard deviation.

The dependences displayed in Fig. 4 clearly indicate that cholesterol acts differently in PGPC containing bilayers compared to the pure POPC ones. The overall drop of the diffusion coefficient in the PGPC containing bilayers is smaller for both the oxidized and non-oxidized moieties compared to the PGPC free bilayer. This effect was confirmed also by the additional independent technique of Z-scan FCS.

Our data do not show any measurable differences in the diffusion coefficients of all four investigated systems in the cholesterol free bilayers. It has to be pointed out that the structural properties of the bilayer's main building stone, POPC, did not display any differences in the simulations. Therefore, we conclude that the fluorescent moiety senses the motion of the nearest neighbors, which remains unchanged. Plochberger et al. shows significantly faster diffusion of the oxidized moiety (PGPE-Alexa647) compared to the non-oxidized lipid (DHPE-Bodipy) in a DOPC bilayer. We believe that this discrepancy accounts for different host lipids and different membrane model systems used in the study.

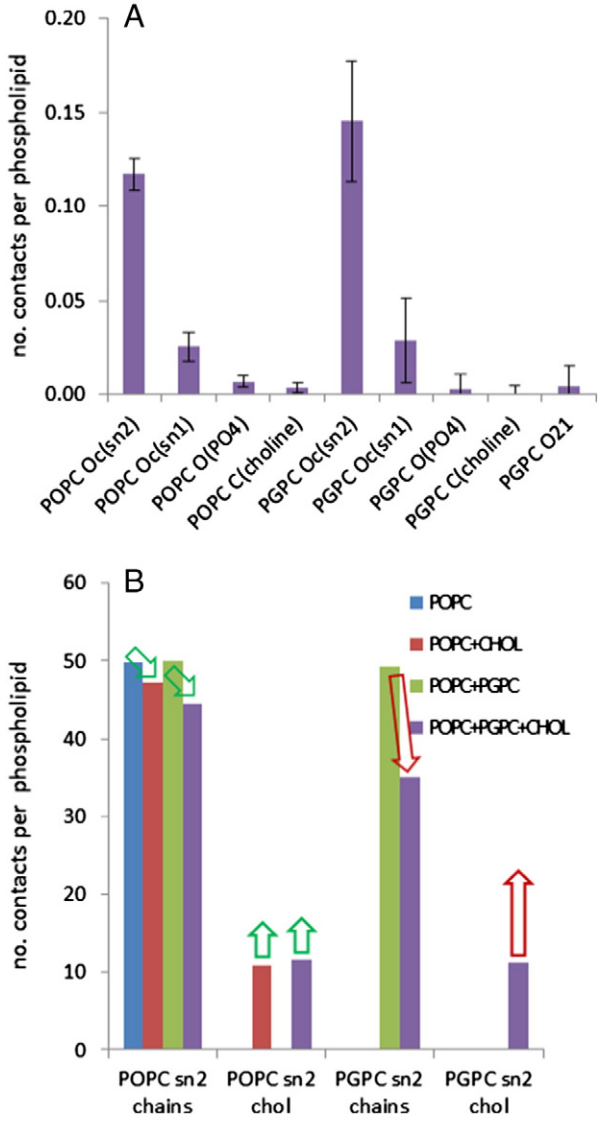

Fig. 5. Number of polar contacts between selected groups in phospholipids and cholesterol calculated per phospholipid molecule (A); and number of non-polar contacts between center carbon atoms of *sn*-2 and either other aliphatic chains ('chains') or non-polar atoms of cholesterol ('chol') calculated per phospholipid molecule (B). Reduction of phospholipid–phospholipid non-polar interaction and elevation of phospholipid–cholesterol contacts are highlighted with arrows. Error bars in (B) are below 1% and are not shown.

To better understand the impact of cholesterol on oxidized membranes, we scrutinized polar and non-polar interactions between cholesterol and other lipids based on simulated MD trajectories. In Fig. 5A, the numbers of polar contacts between cholesterol molecules and selected residues of POPC and PGPC are presented. It is evident that both POPC and PGPC make polar contacts with cholesterol predominantly via the carbonyl groups of their *sn*-2 chains. This can be related with the donation of hydrogen bonds by –OH groups of cholesterol towards the carbonyl oxygen atoms. Polar contacts between cholesterol and both phosphate and choline groups are significantly less frequent. Note that, despite the fact that the *sn*-2 chains of PGPC are reversed, their carbonyl groups still make polar contacts with cholesterol to an extent comparable to that of POPC. It should be taken into account that due to the *sn*-2 chain reorientation in PGPC, most of the carbonyl groups of these chains are located in the region prohibited for –OH group of cholesterol (see a relatively small overlap between the density profile of Oc in PGPC and O_3 in cholesterol in Fig. 2). Based on the overlap of the corresponding density profiles, we estimate that only ~30% of *sn*-2 carbonyl groups of PGPC reside in the region populated by cholesterol –OH group, as compared with ~70% in the case of POPC. As the average number of polar contacts between cholesterol –OH and *sn*-2 carbonyls of both POPC and PGPC *sn*-2 carbonyls are comparable, it can be concluded that effectively *sn*-2 carbonyl groups of PGPC bind cholesterol stronger than the same groups in POPC.

To analyze non-polar lipid–lipid interactions, the numbers of non-polar contacts between the middle carbons of *sn*-2 chains of phospholipids and other non-polar atoms were calculated and are presented in Fig. 5B. As was shown in earlier studies, this quantity is a good measure of non-polar interactions in cholesterol-containing membranes [15]. Upon the addition of cholesterol, the number of non-polar contacts formed between *sn*-2 chains of POPC is slightly reduced, but this reduction is strongly overbalanced by an elevated level of non-polar contacts formed between POPC *sn*-2 and cholesterol (see green arrows in Fig. 5B). This effect is independent on the presence of PGPC in the membrane. Note that the reduction of the number of POPC–POPC contacts in simulated membranes upon the addition of cholesterol is not a dilution effect as the density of cholesterol-containing bilayers is actually higher than that of corresponding cholesterol-free systems (both POPC and POPC + PGPC bilayers undergo lateral compression upon the addition of cholesterol as their area per lipid is reduced). Such an elevated non-polar POPC–cholesterol binding in the membrane core is a manifestation of the condensing effect of cholesterol. Regarding PGPC–cholesterol interactions, the number of non-polar contacts between PGPCs upon cholesterol addition is diminished in a greater extent than in the POPC case and is only partially compensated by the increase of contacts between PGPC and cholesterol (see red arrows in Fig. 5B). Hence, it can be concluded that the condensation effect between cholesterol and PGPC molecules is weaker than that observed for POPC. This effect is also evident in the aforementioned lower reduction of the APL by cholesterol in the PGPC-containing membrane with respect to the pure POPC one. The fact that cholesterol in the PGPC vicinity does not condense the bilayer as effectively as in the case of POPC, explains the smaller overall cholesterol effect on the diffusion coefficient of both labeled lipid moieties.

It is of note that literature available phase diagrams show a transition between liquid disordered phase (L_d) and L_d/liquid ordered (L_o) phase coexistence in POPC/cholesterol mixtures between 15 and 20 mol% of cholesterol. This transition may be responsible for the steep drop in the diffusion coefficient between 10 and 20 mol% of cholesterol that does not occur in the PGPC containing bilayers. This would indicate that PGPC's presence prevents the bilayer from being phase separated. This issue, however, cannot be addressed employing atomistic level simulations due to system size and time limitations. Experimentally we do not observe separated phases at the length scale accessible by diffraction limited light microscopy. In experiment, microscopic phase separation was never observed probably due to limited spatial resolution.

2.3. PGPC presence reflected by EPR measurements and MD simulations

Molecular ordering of the lipid membrane together with motions occurring on the submicrosecond and microsecond timescales can be accessed both by means of MD simulations and experimentally.

EPR spectra are sensitive to subtle changes in lipid chain ordering and have been used in order to study lipid peroxidation [16,17]. We have measured the EPR spectra of three differently localized nitroxide-based spin labels (doxyl radicals). It is well known that the EPR spectrum of a nitroxide spin label consists of three lines as a result of an unpaired $S = 1/2$ electron coupled to a ^{14}N ($I = 1$) nucleus. Line shapes of EPR spectra depend on local order and mobility of the spin label localized within the lipid bilayer. The motions that mainly affect the EPR spectra are trans/gauche isomerization, lipid wobbling and axial rotation. The extent of these motions is changed throughout the membrane leaflet from lower mobility at the headgroup interface towards higher mobility at the more fluid tail region. Placing lipids spin-labeled by the doxyl radical on various carbons of the lipid chain allows for monitoring the effect of oxPLs at various depths of the membrane. The molecular motions in lipid bilayers are highly anisotropic. The short-range order can be characterized by a membrane director. The average position of a molecule with respect to the director is then expressed in terms of the order parameter.

We have monitored the order parameter which indicates ordering and the chain dynamics and microenvironment of the medium in which the spin-probe is incorporated. The apparent lipid acyl-chain order parameters, S, can be determined by measuring the resultant hyperfine splitting of the EPR spectra using the following equation [18]:

$$S = 0.5407\frac{A_{par} - A_{per}}{a_0},\quad a_0 = \frac{A_{par} + 2A_{per}}{3},$$

where A_{par} and A_{per} are the observed hyperfine splitting values measured between the $M_I = +1$ and 0 spectral lines from the parallel and perpendicular oriented EPR spectra, respectively, and a_0 the effective isotropic ^{14}N-hyperfine coupling constant.

The A_{par} value was determined from the maximal outer ^{14}N-hyperfine splitting in the spectra (A_{max}) and A_{per} from the inner hyperfine splitting in the spectra (A_{min}), see Fig. 6.

We have determined the order parameter for three differently located spin probes (5-, 10-, and 16-doxyl PCs) in pure POPC/chol membranes and in membranes with 10% of POPC replaced by PGPC, as a function of cholesterol content (Fig. 7).

Apparently, the spin-probe does not report any significant difference between the oxidized and non-oxidized bilayers at the level of carbon 5, i.e. close to the headgroup region. In the center of the leaflet, carbon 10, order parameter S of the oxidized membrane becomes higher at higher cholesterol content, while in the tail region the trend becomes opposite, i.e. oxidation lowers the structure parameter at carbon 16. Changes in S can be attributed to increased order of the central part of the oxidized membrane at higher cholesterol level and vice versa in the inner part of the leaflet. Most probably the ordering effect is accompanied with decreased mobility.

A parameter analogous to the EPR order parameter, the deuterium order parameter, was obtained by means of MD simulations. The order parameter reports the mobility of the CD_2 group on a lipid chain. It is obtained according to the formula:

$$S = {}^{1}\!/_{2}\left\langle 3\left\langle \cos^2\theta\right\rangle - 1\right\rangle,$$

where θ is the angle between a C–D bond and the membrane director, and the angular brackets stand for averaging over the two C–D bonds, all lipids in simulation and time. The simulation, in accordance with the EPR data, predicts higher ordering (less motion) of the POPC *sn*-1 chain in the center of the leaflet at high cholesterol content, while the tail region is almost unaffected (see Fig. S3 in the Supporting information).

Higher ordering of the center of the membrane leaflet most probably results from the specific cholesterol interaction with the oxidized chain's carbonyl. It seems that the oxPL, with its missing chain now replaced by a cholesterol molecule, fits within the POPC membrane in a way that is more stable than a POPC molecule itself. The slightly lower EPR order parameter in the tail region of the oxidized bilayer is most probably due to the fact that the PGPC molecule is shifted outwards. This results in the fact that even the non-oxidized *sn*-1 chains do not reach the inter-leaflet area as the *sn*-1 chains of POPC do and by that

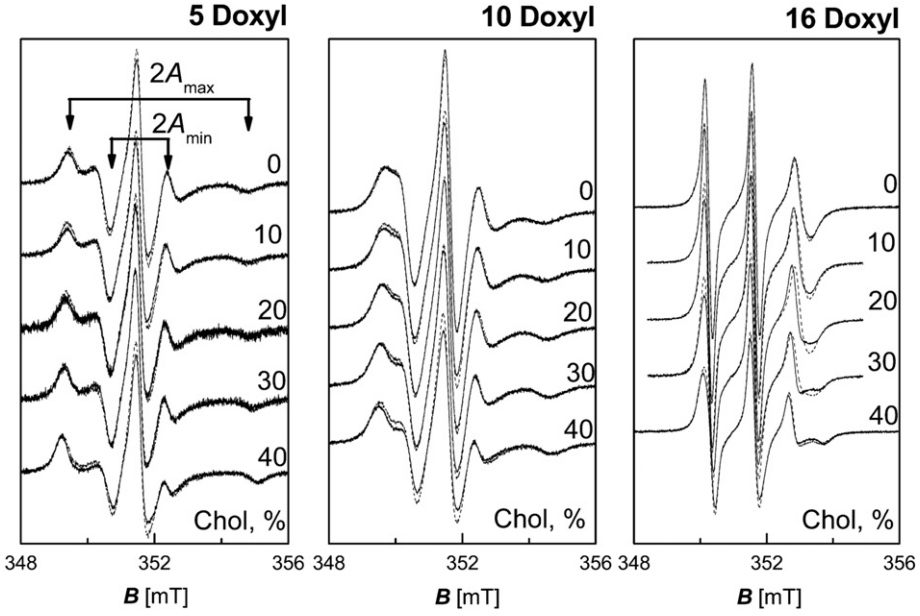

Fig. 6. X-band EPR spectra measured for 5-, 10-, and 16-doxyl PCs. Solid lines are experimental spectra from pure POPC/chol membranes, dashed lines are from membranes with 10% of POPC replaced by PGPC.

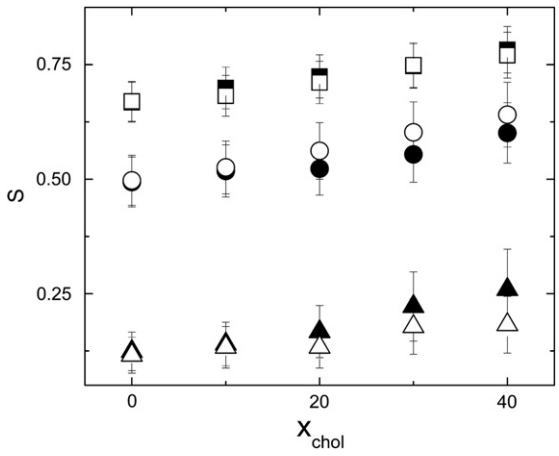

Fig. 7. Order parameter, *S*, for three 5- (square), 10- (circle), and 16- (triangle) doxyl PCs in pure POPC/chol membranes (full symbols) and in membranes with 10% of POPC replaced by PGPC (open symbols) as a function of cholesterol content.

do not participate in the POPC interdigitation. This might provide more space for the motion of the doxyl group at carbon 16.

It has to be kept in mind that the probe for the EPR experiment is large and thus disturbs the bilayer when compared to the deuterium atom in the case of the NMR experiment or the simulation in our work. Moreover, also the timescale of the EPR experiment and the simulation slightly differ, therefore the approaches are not fully comparable. Indeed, despite the qualitative agreement, there is no quantitative correspondence between the order parameter from EPR experiment (Fig. 7) and that calculated in MD simulations (Fig. S3) Nonetheless, the EPR experimental outcome as well as the MD simulation predicting higher lipid ordering in the center of the leaflet can be further supported by the work of Volinsky et al. [19] stating remarkably lowered polarity of the central leaflet in the presence of oxPLs.

3. Materials and methods

3.1. Chemicals

1-Palmitoyl-2-oleoyl-*sn*-glycero-3-phosphocholine (POPC), 1-palmitoyl-2-oleoyl-*sn*-glycero-3-phosphoethanolamine (POPE), 1-palmitoyl-2-glutaryl-sn-glycero-3-phosphocholine (PGPC), cholesterol, 1,2-dipalmitoyl-*sn*-glycero-3-phosphoethanolamine-N-(cap biotinyl) (biotinyl Cap PE), 1-palmitoyl-2-stearoyl-(5-doxyl)-*sn*-glycero-3-phosphocholine (5-doxyl PC), 10-doxyl PC and 16-doxyl PC were purchased from Avanti Polar Lipids (Alabaster, AL, U.S.A.) and used without further purification. POPE was covalently labeled by ATTO488-NHS-ester (Siegen, Germany) and purified by adsorption chromatography on silica gel column Kieselgel 60 (Merck, Whitehouse Station, NJ, U.S.A.) in chloroform/methanol/water (60/25/4) eluent. Bodipy-labeled PGPC was synthesized as described elsewhere [20].

3.2. Sample preparation

Giant unilamellar vesicles (GUVs) for fluorescence microscopy were prepared by the electroformation method using titanium chambers as described by Angelova et al. [21] Lipid mixtures were made from stock solutions in chloroform. The overall amount of all lipids (100 nmol in approximately 200 μl of chloroform) together with the labeled lipids was spread onto two hollowed titanium plates which were placed on a heater plate at approximately 50 °C to facilitate solvent evaporation, and subsequently put under high vacuum for at least 1 h for evaporation of remaining traces of solvent. The lipid-coated plates were assembled using one layer of Parafilm for insulation [22]. The electroswelling chamber was filled with 1 ml preheated sucrose solution (100 mM sucrose, and osmolarity of 103 mOsm/kg) and sealed with Parafilm. An alternating electrical field of 10 Hz rising from 0.02 V to 1.1 V (peak-to-peak voltage) in the first 45 min was applied and then kept at 1.1 V for additional 2.5 h at 55 °C, followed by 30 min of 4 Hz and 1.3 V to detach the formed liposomes. Finally, the GUVs were placed to a microscopy chamber containing glucose buffer (~80 mM glucose, 10 mM HEPES and 10 mM NaCl, pH 7.2) with an osmolarity of 103 mOsm/kg. All lipid mixtures contained 2 mol% of biotinyl Cap PE for immobilization of GUVs on BSA-biotin/streptavidin coated bottom of the chamber.

Multilamellar vesicles (MLVs) for EPR experiments were prepared as follows. Chloroform solutions of appropriate lipids were dried under nitrogen and subsequently put to the desiccator for 1 h. The lipid film was hydrated in a HEPES buffer (10 mM HEPES, 150 mM NaCl, 2 mM EDTA, pH = 7). The overall lipid concentration was 10 mM, the amount of the appropriate doxyl label was 0.5 mol%.

3.3. Fluorescence microscopy

2-Foci fluorescence correlation spectroscopy (2f FCS) has been carried out on a home built confocal microscope consisting of an inverted confocal microscope body IX71 (Olympus, Hamburg, Germany). For excitation, the 60-ps pulsed 470 nm diode laser head LDH-P-C-470B (Picoquant, Berlin, Germany) was used. The polarization of the laser light was periodically rotated with an electro-optic amplitude modulator (EO-AM-R-20-C4, Thorlabs, Dachau, Germany) so that the polarization of every pulse was orthogonal with respect to the previous one. The laser pulses are synchronized with the sine voltage wave imposed on the modulator using a DA4300 30MS/s arbitrary waveform generator (Acquitek, Massy, France). Its voltage output was further amplified.

The laser light was coupled to a polarization maintaining a single mode optical fiber and at the output re-collimated with an UPlanSApo 10×, N.A. 0.4 objective lens (Olympus) so that the light beam underfilled the principal microscope objective lens (60×, W, 1.2 N.A., Olympus) and the size of the focal spot was enlarged compared to the diffraction limited situation. The light was up-reflected to the objective with a Z470rdc dichroic mirror (Chroma, Rockingham, VT). Underneath the objective lens, a Nomarski prism (U-DICTHC, Olympus) was placed in such a way that its axes were aligned with the orthogonal polarization of the laser pulses. Through this, the pulses of different polarization were focused into two spatially shifted, overlapping foci. The distance between the foci was precisely determined by scanning of sub-diffraction sized fluorescence beads and it uniquely depends on the prism used.

The emission light was focused on a 150 μm-pinhole and after having been re-collimated it was split onto two single-photon avalanche diodes (Micro-Photon Devices, Bolzano, Italy). Emission filters (HQ515/50) were placed in front of the detectors.

The auto- and cross-correlation functions (ACFs, CCFs) corresponding to the fluorescence intensity traces in the individual foci were calculated and fit in Matlab (Mathworks, Natick, MA) using home-written scripts that take into account the point spread function (PSF) and the mathematical model of 2-dimensional diffusion described by Dertinger et al. [23].

Z-scan FCS has been performed on the same microscope as the 2fFCS experiments with several alterations: i) the Nomarski prism was removed, ii) laser light after having passed the optical fiber was re-collimated using UPlanSApo 4× (N.A. 0.16) lens so that the principal objective lens became exactly filled, i.e. the size of the diffraction spot is diffraction limited, and iii) the pinhole size was reduced to 50 μm. The upper membrane of the GUV was placed approximately 1 μm below the laser focus and moved in 150-nm steps to 1 μm above the focus. At every position, a 60-second fluorescence intensity measurement was performed, ACFs calculated and fitted with a model accounting for one diffusion component [24]. The fitting read-out parameters: average number of particles and diffusion time were plotted as a

function of membrane-focus position, minimum diffusion time was then identified and converted to the diffusion coefficient. The size of the focus was chosen so that the diffusion coefficient for the cholesterol free bilayers was in accord with the value obtained by 2fFCS. 2fFCS thus served as a calibration.

3.4. EPR spectroscopy

The X-band room temperature continuous wave EPR spectra were measured using a Bruker X-/Q-band E580 FT/CW ELEXSYS spectrometer. For the measurements the ER 4122 SHQE SuperX High-Q cavity with TE_{011} mode was used. The samples were placed into quartz tubes with a diameter of 2 mm. The experimental parameters were: microwave frequency 9.876 GHz, microwave power 4.743 mW, modulation frequency 100 kHz, modulation amplitude 0.2 mT, and the conversion time 60 ms.

3.5. Molecular dynamics simulations

Classical molecular dynamics simulations were employed to study lipid bilayers with varying lipid compositions. The Berger's non-polarizable united-atom force field was used for description of lipids [25] and water molecules were modeled with the SPC model, for which the lipid force field was derived [26]. Oxidized PGPC lipids were described employing parameters developed based on the Berger's force field by the Tieleman's group [9], and the cholesterol force field of Holtje and co-workers was employed [27]. Sodium cation parameters were taken from the GROMACS force field [28]. Fifteen lipid membranes, each containing 128 phospholipids (with varying POPC to PGPC molar ratio) with cholesterol molecules were simulated. Each membrane was hydrated by over 6000 water molecules resulting in a phospholipid to lipid molar ratio of over 40. Sodium cations were added to the water phase in the case of PGPC-containing systems in order to neutralize the negative charge of PGPC. Each system was simulated for 100 ns, in two cases the simulation time was extended to 200 ns. The total simulation time of all systems was equal to 1700 ns. A convergence of the APL was used as an equilibration criterion. The trailing 50 ns of each trajectory was used for analysis. Compositions of simulated systems are specified in Table S1 and a typical view of the simulation box is presented in Fig. S1 in the Supporting information. Four trajectories, each representing one type of lipid composition, were selected for detailed analysis: POPC (100 mol%), POPC + PGPC (POPC with 9 mol% PGPC), POPC + chol (POPC with 23 mol% of cholesterol), and POPC + PGPC + chol (POPC with 7 mol% PGPC and 23 mol% of cholesterol). Periodic boundary conditions were employed with typical size of the simulation box of $6.3 \times 6.3 \times 9.3$ nm^3. The cutoff of 1 nm was employed for both Lennard–Jones and short-range electrostatic interactions, and the long-range electrostatics was accounted for by employing the particle-mesh Ewald method [29]. The semi-isotropic Parrinello–Rahman pressure coupling scheme was used with the pressure of 1 bar and the coupling constant of 2 ps [30]. The temperature of 310 K was controlled independently for lipids and the water phase via Nose–Hoover thermostat algorithm with the 1 ps coupling constant [31]. Bond lengths in lipids were kept constant employing the LINCS algorithm [32] and rigidity of water molecules was achieved by using the SETTLE method [33]. Equations of motion were integrated with a 2 fs time step. Simulations were performed employing the GROMACS 4.5.5 software package [28].

Polar contacts between cholesterol and phospholipids were calculated as an average number of neighbors up to the distance of 0.3 nm between the cholesterol oxygen atoms and the given atoms of lipid molecules per one phospholipid. The value was averaged along the equilibrated part of the trajectory, and the standard deviation is reported as the error value. Non-polar contacts between phospholipid chains were calculated as an average number of neighbors up to the distance of 0.7 nm between the central carbon atoms of sn-2 lipid chains per phospholipid molecule. Similarly, an average number of central carbon atoms of phospholipid chains and all carbon atoms of cholesterol per phospholipid were used for calculation of non-polar contacts between phospholipids and cholesterol. Contact values were averaged along the equilibrated part of the trajectory, and the standard deviation is reported as the error value. The cutoffs for contact calculations are based on the positions of the first minima in the corresponding radial distribution functions and are the same as those employed in Ref. [15].

4. Conclusion

In this work, we present a detailed portrait of physical changes that the presence of oxPLs imposes on a model phospholipid bilayer. While the structural arrangement of the non-oxidized moiety, POPC, remains unaffected when PGPC appears, the PGPC itself organizes in a very distinct manner. The PGPC molecule is pushed out of the bilayer center and its truncated chain loops back to the headgroup area. The partial chain reversal is most probably responsible for the two populations of flat-laying and straight-staying choline residues in PGPC.

The very different positions and behaviors of PGPC do not seem to significantly affect both the long- and short- timescale dynamics of a cholesterol free membrane. The oxidized membrane, however, interacts differently with cholesterol. While in the non-oxidized bilayer cholesterol has a condensing affect, in the PGPC containing bilayer cholesterol preferentially fills the void space and in this way “heals” the oxidation-caused damage. The preference of cholesterol for the carbonyl of the fully reversed truncated chain together with the fact that cholesterol ceases to have a condensing effect suggests a higher capacity of the oxidized bilayer to accommodate cholesterol without changing its physical properties. This is demonstrated by the lower impact of cholesterol on the diffusion coefficient of lipid moieties in oxidized bilayers.

In the oxidized bilayer, despite more space available, the distribution of cholesterol tilt-angles becomes slightly narrower compared to the non-oxidized bilayer, which suggests that cholesterol indeed specifically interacts with the oxPLs. This is translated into higher values of EPR and deuterium order parameter in the central part of the bilayer leaflet indicating higher ordering and less motion in that area.

To sum up, phospholipid membranes that underwent the oxidation process are stabilized by cholesterol, which preferentially “heals” the oxidative damage.

Acknowledgement

Financial support was provided by the Czech Science Foundation (P208/12/G016 to M.S. R.S., A.O., M.H.) and the Ministry of Education, Youth and Sports of the Czech Republic (LH 13259 KONTAKT to M.A. and J.H.). Moreover the Academy of Sciences for the Praemium Academie Award is acknowledged (M.H.). D.S. and A.D. acknowledge the support within the framework of large infrastructure SAFMAT (Project No. CZ.2. 13/3.1.00/22132).

Appendix A. Supplementary data

Compositions of simulated lipid bilayers. Typical snapshot of the simulation box. Density profiles calculated in simulated membranes. Deuterium order parameter calculated for various carbons along the *sn*-1 chain in POPC in the oxidized and non-oxidized bilayers for different cholesterol levels. Supplementary data associated with this article can be found, in the online version, at http://dx.doi.org/10.1016/j.bbamem.2014.02.006.

References

[1] G.O. Fruhwirth, A. Loidl, A. Hermetter, Oxidized phospholipids: from molecular properties to disease, Biochim. Biophys. Acta (BBA) - Mol. Basis Dis. 1772 (2007) 718–736.

[2] M.H. Brodnitz, Autoxidation of saturated fatty acids — a review, J. Agric. Food Chem. 16 (1968) 994–999.
[3] N.A. Porter, S.E. Caldwell, K.A. Mills, Mechanisms of free-radical oxidation of unsaturated lipids, Lipids 30 (1995) 277–290.
[4] L.G. Wood, P.G. Gibson, M.L. Garg, Biomarkers of lipid peroxidation, airway inflammation and asthma, Eur. Respir. J. 21 (2003) 177–186.
[5] V.N. Bochkov, Inflammatory profile of oxidized phospholipids, Thromb. Haemost. 97 (2007) 348–354.
[6] V.N. Bochkov, A. Kadl, J. Huber, F. Gruber, B.R. Binder, N. Leitinger, Protective role of phospholipid oxidation products in endotoxin-induced tissue damage, Nature 419 (2002) 77–81.
[7] U. Stemmer, A. Hermetter, Protein modification by aldehydophospholipids and its functional consequences, Biochim. Biophys. Acta - Biomembr. 1818 (2012) 2436–2445.
[8] H. Khandelia, O.G. Mouritsen, Lipid gymnastics: evidence of complete acyl chain reversal in oxidized phospholipids from molecular simulations, Biophys. J. 96 (2009) 2734–2743.
[9] J. Wong-Ekkabut, Z.T. Xu, W. Triampo, I.M. Tang, D.P. Tieleman, L. Monticelli, Effect of lipid peroxidation on the properties of lipid bilayers: a molecular dynamics study, Biophys. J. 93 (2007) 4225–4236.
[10] L. Beranova, L. Cwiklik, P. Jurkiewicz, M. Hof, P. Jungwirth, Oxidation changes physical properties of phospholipid bilayers: fluorescence spectroscopy and molecular simulations, Langmuir 26 (2010) 6140–6144.
[11] B. Plochberger, T. Stockner, S. Chiantia, M. Brameshuber, J. Weghuber, A. Hermetter, P. Schwille, G.J. Schutz, Cholesterol slows down the lateral mobility of an oxidized phospholipid in a supported lipid bilayer, Langmuir 26 (2010) 17322–17329.
[12] M. Lis, A. Wizert, M. Przybylo, M. Langner, J. Swiatek, P. Jungwirth, L. Cwiklik, The effect of lipid oxidation on the water permeability of phospholipids bilayers, Phys. Chem. Chem. Phys. 13 (2011) 17555–17563.
[13] R. Volinsky, R. Paananen, P.K.J. Kinnunen, Oxidized phosphatidylcholines promote phase separation of cholesterol–sphingomyelin domains, Biophys. J. 103 (2012) 247–254.
[14] K. Sabatini, J.P. Mattila, F.M. Megli, P.K.J. Kinnunen, Characterization of two oxidatively modified phospholipids in mixed monolayers with DPPC, Biophys. J. 90 (2006) 4488–4499.
[15] T. Rog, M. Pasenkiewicz-Gierula, I. Vattulainen, M. Karttunen, Ordering effects of cholesterol and its analogues, Biochim. Biophys. Acta - Biomembr. 1788 (2009) 97–121.
[16] F.M. Megli, L. Russo, E. Conte, Spin labeling EPR studies of the properties of oxidized phospholipid-containing lipid vesicles, Biochim. Biophys. Acta - Biomembr. 1788 (2009) 371–379.
[17] P. Jurkiewicz, A. Olzynska, L. Cwiklik, E. Conte, P. Jungwirth, F.M. Megli, M. Hof, Biophysics of lipid bilayers containing oxidatively modified phospholipids: insights from fluorescence and EPR experiments and from MD simulations, Biochim. Biophys. Acta - Biomembr. 1818 (2012) 2388–2402.
[18] D. Marsh, Electron spin resonance: spin labels, in: E. Grell (Ed.), Membrane Spectroscopy, Springer-Verlag, Berlin, 1981, pp. 51–142.
[19] R. Volinsky, L. Cwiklik, P. Jurkiewicz, M. Hof, P. Jungwirth, P.K.J. Kinnunen, Oxidized phosphatidylcholines facilitate phospholipid flip-flop in liposomes, Biophys. J. 101 (2011) 1376–1384.
[20] J.A.M. Rasmussen, A. Hermetter, Chemical synthesis of fluorescent glycero- and sphingolipids, Prog. Lipid Res. 47 (2008) 436–460.
[21] M.I. Angelova, S. Soleau, P. Meleard, J.F. Faucon, P. Bothorel, Preparation of giant vesicles by external ac electric-fields — kinetics and applications, Trends Colloid Interface Sci. VI 89 (1992) 127–131.
[22] V. Weissig (Ed.), Liposomes: methods and protocols, Biological Membrane Models, vol. 2, Humana Press, New York, 2010.
[23] T. Dertinger, V. Pacheco, I. von der Hocht, R. Hartmann, I. Gregor, J. Enderlein, Two-focus fluorescence correlation spectroscopy: a new tool for accurate and absolute diffusion measurements, ChemPhysChem 8 (2007) 433–443.
[24] A. Benda, M. Benes, V. Marecek, A. Lhotsky, W.T. Hermens, M. Hof, How to determine diffusion coefficients in planar phospholipid systems by confocal fluorescence correlation spectroscopy, Langmuir 19 (2003) 4120–4126.
[25] O. Berger, O. Edholm, F. Jahnig, Molecular dynamics simulations of a fluid bilayer of dipalmitoylphosphatidylcholine at full hydration, constant pressure, and constant temperature, Biophys. J. 72 (1997) 2002–2013.
[26] H.J.C. Berendsen, J.P.M. Postma, W.F.v. Gunsteren, J. Hermans, Interaction Models for Water in Relation to Protein Hydration. Intermolecular Forces, D. Reidel Publishing Company, Dodrecht, 1981. 331–342.
[27] M. Holtje, T. Forster, B. Brandt, T. Engels, W. von Rybinski, H.D. Holtje, Molecular dynamics simulations of stratum corneum lipid models: fatty acids and cholesterol, Biochim. Biophys. Acta - Biomembr. 1511 (2001) 156–167.
[28] B. Hess, C. Kutzner, D. van der Spoel, E. Lindahl, GROMACS 4: algorithms for highly efficient, load-balanced, and scalable molecular simulation, J. Chem. Theory Comput. 4 (2008) 435–447.
[29] U. Essmann, L. Perera, M.L. Berkowitz, T. Darden, H. Lee, L.G. Pedersen, A smooth particle mesh Ewald method, J. Chem. Phys. 103 (1995) 8577–8593.
[30] M. Parrinello, A. Rahman, Polymorphic transitions in single-crystals — a new molecular-dynamics method, J. Appl. Phys. 52 (1981) 7182–7190.
[31] S. Nose, A molecular-dynamics method for simulations in the canonical ensemble, Mol. Phys. 52 (1984) 255–268.
[32] B. Hess, H. Bekker, H.J.C. Berendsen, J.G.E.M. Fraaije, LINCS: a linear constraint solver for molecular simulations, J. Comput. Chem. 18 (1997) 1463–1472.
[33] R.W. Hockney, S.P. Goel, J.W. Eastwood, Quiet high-resolution computer models of a plasma, J. Comput. Phys. 14 (1974) 148–158.